THE HIGH TEMPERATURE CREEP DEFORMATION OF Si_3N_4-$6Y_2O_3$-$2Al_2O_3$

J. A. Todd[1] and Zhi-Yue Xu[2]

1. Assistant Professor, Departments of Materials Science and Mechanical Engineering, University of Southern California, Los Angeles, CA 90089-0241, USA

2. Research Assistant, Department of Materials Science, University of Southern California, Los Angeles, CA 90089-0241, USA

ABSTRACT

The creep properties of silicon nitride containing 6 wt% yttria and 2 wt% alumina have been determined in the temperature range 1573 to 1673 K. The stress exponent, n, in the equation $\dot{\varepsilon} \propto \sigma^n$, was determined to be 2.00 $\pm$ 0.15 and the true activation energy was found to be 692 $\pm$ 25 kJ mol^{-1}. Transmission electron microscopy studies showed that deformation occurred in the grain boundary glassy phase accompanied by microcrack formation and cavitation. The steady state creep results are consistent with a diffusion controlled creep mechanism involving nitrogen diffusion through the grain boundary glassy phase.

1. INTRODUCTION

Advanced processing techniques, such as sintering, gas-pressure sintering, post-sintering and hot isostatic pressing (HIP) are currently being developed to improve the mechanical properties of dense silicon nitride (Si_3N_4) [1]. Achievement of full density in both sintered silicon nitride (SSN) and hot isostatically pressed silicon nitride (HIPSN) requires the presence of additives to promote densification by liquid phase sintering [2-4]. Three groups of additives have been used [1,5-7]: (a) oxides (MgO, Y_2O_3, Y_2O_3 + Al_2O_3), which do not form solid solutions with Si_3N_4; (b) oxide and non-oxide additives (BeO, $BeSiN_2$, Al_2O_3 + AlN, AlN + Y_2O_3) which do form solid solutions with Si_3N_4; and (c) non-oxide additives (Be_3N_2, ZrN, ZrC, Zr + AlN, Mg_3N_2) which give higher viscosity grain boundary phases. Additives such as MgO result in a continuous, amorphous, magnesium silicate intergranular phase [8-11], whilst those containing Y_2O_3-Al_2O_3 additions may possess both crystalline and amorphous grain boundary phases [12-15]. The presence of a glassy grain boundary phase is deleterious to both the room temperature and elevated temperature mechanical properties of silicon nitride.

The creep properties of dense silicon nitride, which are mainly controlled by grain boundary sliding along the amorphous phase, can be improved by: (1) increasing the viscosity of the grain boundary phase; (2) crystallization of the grain boundary phase; and (3) production of high aspect ratio beta-Si_3N_4 grains, favored by high viscosity melts [1,16-19]. Hence, additives such as Y_2O_3, which give a higher viscosity grain boundary phase, generally result in lower creep rates than for MgO-doped silicon nitride [20]. However, a second oxide additive, Al_2O_3, is frequently combined with Y_2O_3, to avoid problems of reduced densification rates and higher densification temperatures, produced by

the single refractory oxide additive [21,22].

To date, there have been few reports of the elevated temperature properties of silicon nitride containing refractory and rare-earth oxides [1,19,20, 23-26]. The present study was, therefore, undertaken to investigate (a) the creep behavior of Si_3N_4-6Y_2O_3-2Al_2O_3 (wt%) processed by a two stage gas-pressure sintering technique; (b) the role of the grain boundary phase; and (c) the rate controlling mechanism for steady state creep.

2. EXPERIMENTAL PROCEDURES

The material used in this study contained 92 wt% GTE SN 502 powder, 6 wt% Molycorp Y_2O_3 powder amd 2 wt% Linde Al_2O_3 powder, all <1 μm in size. The powders were dry-ball milled for 24 hours using sintered Si_3N_4 grinding media, then blended with a binder, pelletized and injection molded into test bars 50.8 mm x 6.4 mm x 3.2 mm. Following binder burnout, the specimens were sintered using a two stage gas pressure sintering technique. The pre-sintering stage, conducted at a nitrogen pressure of 0.6 MPa (90 ksi) for 4 hours at 2123 K, was required to remove open porosity. In the second stage, the temperature and pressure were raised to 2173 K and 10.3 MPa (1500 psi) nitrogen for 2 hours to complete the densification cycle. (It should be noted that sintering temperatures are limited to 2093 K with 0.1 MPa (atmospheric pressure) N_2. The use of higher N_2 pressures permits sintering at higher temperatures (up to 2473 K for 10 MPa N_2) and the use of smaller quantities of refractory additives.)

Specimens for creep testing were nominally 25 mm x 3 mm x 3 mm. They were deformed in four point flexure with an outer span of 19 mm and an inner span of 6.4 mm. High purity sapphire rods were used for pivot points. The displacement of the inner pivot points was monitored with a linear variable differential transformer and chart recorder. Tests were conducted in an air environ-

ment at constant stresses between 10.4 MPa and 52 MPa in the temperature range 1573 K to 1673 K. The furnace was allowed to stabilize for 90 minutes at the test temperature before commencing the creep tests. Stress and strain data were computed for the four-point bend specimen from the load-displacement data using the procedure developed by Hollenberg et al. [27].

Scanning electron micrographs were taken from both the polished and etched tensile surfaces and the fracture surfaces of the creep tested samples. Transmission electron microscopy samples were taken from the as-received material and the tensile face of partially deformed creep specimens. The samples were thinned by ion beam milling and examined in a Philips 430 transmission electron microscope operated at 300 kV.

3. RESULTS

3.1 Creep Data

Creep strain (%) versus time data, showing normal primary, secondary and tertiary regions are shown in Fig. 1 for a sample tested at 1673 K and a stress of 36.4 MPa. Strain rate data versus strain are summarized in Fig. 2 for specimens tested at 1673 K and stresses in the range 10.4 to 52 MPa. A well defined steady state region was observed for strains above 1%, at all stresses above 19.9 MPa. However, at 10.4 MPa the strain rate continued to decrease with increasing strain and steady state behavior was not observed. It should be noted that rupture times of 0.4 - 1.2 h and 1.5 - 5.3 h were observed for specimens tested at 52 Mpa and 36.1 MPa, respectively, whereas for 19.9 and 10.4 MPa the tests were stopped, prior to rupture, after approximately 22 h.

3.2 Stress Exponent

Steady state strain rate data are plotted versus stress, for temperatures of 1673 K, 1623 K and 1573 K, in Fig. 3. The error bars for the stress, 10.4

MPa, at 1673 K indicate the strain rates between a strain level of 1.5% and the strain level corresponding to the end of the test. Inspection of Fig. 3 reveals that the creep behavior of Si_3N_4-$6Y_2O_3$-$2Al_2O_3$ is associated with a stress exponent of 2.00 ± 0.15.

3.3 Activation energy for creep deformation

The apparent activation energy for creep deformation was determined from the secondary creep rate versus applied stress data shown in Fig. 3, for an applied stress of 50 MPa. These steady state creep data are plotted against 1/T in Fig. 4. From the slope of the line in Fig. 4, an apparent activation energy of 700 ± 25 kJ mol^{-1} was determined.

3.4 Microstructural observations

Transmission electron micrographs of the as-sintered material are shown in Figs. 5(a) and 5(b). The material is predominantly β-Si_3N_4 with an average grain diameter of 0.7 μm. The grain labelled A in Fig. 5(a) has an aspect ratio greater than 5. Equiaxed grain sizes up to approximately 2.5 μm can be seen in Fig. 5(a) suggesting that some grain growth may have occurred during the sintering treatment. The silicon nitride grains are surrounded by a continuous glassy phase, which was shown by energy dispersive X-ray spectroscopy (EDX) to contain silicon and yttrium (dark region, labelled B in Fig. 5(b)).

Scanning electron micrographs of the specimen creep deformed for 1.5 h at 1673 K and an applied stress of 72.7 MPa are shown in Fig. 6. The polished, unetched, tensile surface in Fig. 6(a) shows the development of cracks and cavities along boundaries perpendicular to the applied stress. Figure 6(b) shows the thermally etched side of the specimen, adjacent to the fracture surface, with a region of incomplete sintering at the bottom right. The fracture surface, containing many small voids and cracks is shown in Figs. 6(c) and 6(d).

Transmission electron micrographs of the specimen creep tested for 22.4 hours at 1673 K and a stress of 19.9 Mpa are presented in Fig. 7. Evidence of grain boundary sliding (labelled A) and occasional dislocation activity (labelled B) can be seen in Fig. 7(a) . The glassy phase in Fig. 7(a) is seen to contain small (0.04 μm) light areas in a dark matrix (labelled C). Tilting of the specimen did not reveal a change in contrast, indicating that these regions were not crystalline. Careful study of several regions, which were all found to be amorphous, and comparison of the micrographs with those of Leng-Ward and Lewis [28], suggested that the glass had separated into two amorphous phases during the creep test. Similar regions were only occasionally observed in the as-received specimen. It should be noted that there appeared to be evidence of phase separation immediately adjacent to the silicon nitride grains in several cases. An alternative explanation for the two phase regions might be the presence of gas bubbles, if the reduction of nitrogen ions to nitrogen gas were to occur at the Si_3N_4/glass interface.

Small crystalline regions, with only the elements Si and Y being detected by EDX, were also observed in the creep tested sample. A more detailed study of the phases present is currently in progress, but it was clear that the majority of the grain boundary phase observed in the present study was amorphous.

The formation of creep cavities at triple points and deformation of the glassy phase are clearly seen in Fig. 7(b). Meniscus formation can be seen at the regions labelled D in Fig. 7(b).

3.5 X-ray diffraction data

X-ray diffraction data were taken from the specimen creep tested for 22.4 hours at 1673 K and a stress of 19.9 MPa. These data confirmed the presence of β-Si_3N_4 with a trace of α-Si_3N_4, and X-ray lines could also be matched with

yttrium aluminum garnet [1/2($3Y_2O_3$.$5Al_2O_3$)]; aluminum yttrium oxides, $YAlO_3$ and $Al_5Y_3O_{12}$; and yttrium silicon oxide nitride, Si_3N_4.Y_2O_3. A detailed transmission electron microscopy study is now in progress to unambiguously identify the crystalline phases present.

3.6 Grain size measurements

Grain size measurements, from the transmission electron micrographs, were made for samples taken from the as-sintered material and the specimen crept at 19.9 MPa for 22.4 hours at 1673 K. The average grain width increased from 0.7 $\pm$ 0.25 μm in the as-sintered material to 1.0 $\pm$ 0.25 μm in the crept material. There was insufficient data in the transmission electron micrographs to obtain accurate aspect ratio measurements. The limited data collected suggests that grain growth was not a major factor in the short term creep tests.

4. DISCUSSION

4.1 Creep data

With the exception of the 10.4 Mpa test at 1673 K, all the creep curves obtained for stresses above 19.9 MPa in the temperature range 1573 - 1673 K exhibited primary, secondary and tertiary creep regions. This is in agreement with (a) data reported by Heinrich and Böhmer [20] for four point bend tests of hot isostatically pressed yttria-doped silicon nitride in air at 1623 K, and (b) other comprehensive studies of creep in hot pressed silicon nitride [1,17,29,30]. In contrast, Arons and Tien [31] reported that for tensile creep tests of hot pressed silicon nitride containing magnesia additives (NC-132) no steady state creep was observed and the strain followed power law time kinetics. Similarly, Bouarroud et al. [25] reported a very long primary creep stage in creep tests of Si_3N_4-$25SiO_2$-$5Y_2O_3$ (mol%). However, it should be noted that both Arons and Tien and Bouarroud et al. conducted their tests at

lower temperatures (1450 K to 1533 K) than the studies reported above (1573 K-1673 K). Their observations agree with those of Davies and Sinha-Ray [32], who noted that decreasing the test temperature increased the extent of primary creep in polycrystalline alumina.

4.2 Stress Exponent

The observations of deformation in the glassy phase at grain boundaries together with wedge cracks and cavitation suggests a viscoelastic mechanism, characterised by a stress exponent, n = 1. In the present study, a stress exponent of 2.0 was determined for Si_3N_4-$6Y_2O_3$-$2Al_2O_3$ in agreement with data for SiAlON and silicon nitrides [17-19,29-31,33-42]. This apparent discrepancy has been reconciled by Evans and Rana [43], who developed statistical models for the creep strain and the failure time of high temperature ceramics in the presence of grain boundary cavitation. Their model predicts a stress exponent of 2 for materials with a continuous grain boundary phase, in which cavities are formed by the viscous flow of the boundary phase in the presence of both an external stress and boundary sliding displacements.

4.3 Activation Energy for Creep Deformation

The steady state creep deformation of ceramic materials can be represented by an equation of the following form [23]:

$$\dot{\varepsilon} = \frac{AGbD}{kT} (b/d)^p (\sigma/G)^n \qquad (1)$$

where, $\dot{\varepsilon}$ = strain rate, G = shear modulus, b = Burgers' vector, k = Boltzmann's constant, T = absolute temperature, D = diffusivity (= $D_o \exp [-Q/(RT)]$), D_o = constant, Q = activation energy of the appropriate diffusion process, R = gas constant, d = grain size, p = inverse grain size exponent, σ = applied stress and n = stress exponent.

The activation energy determined from the Arrhenius plot of strain rate

against reciprocal temperature in Fig. 4 is given by the expression:

$$Q_a = - R \partial \ln \dot{\varepsilon} / \partial (1/T) \quad (2)$$

In order to identify the rate controlling mechanism, the true activation energy, given by the following expression, must be determined.

$$Q_t = - R \partial \ln D / \partial (1/T) \quad (3)$$

Combining equations (1) to (3) gives the following relationship between the true and apparent activation energies.

$$Q_t = Q_a + RT - [(1 - n)RT^2/G] \, dG/dT \quad (4)$$

The shear modulus at temperature can be determined from the relationship:

$$G_T = G_o + (dG/dT)T \quad (5)$$

Shear modulus data as a function of temperature in air have been determined for silicon nitride by several authors [29,44-47]. Kossowsky et al. [29], showed that the shear modulus varied linearly with temperature up to 1473 K, (giving a slope $(dG/dT) = -8.97$ MPa K^{-1} and a value of $G_o = 1.24 \times 10^5$ MPa) but decreased more rapidly above 1473 K. Similar values can be determined from the Young's modulus data reported by Bonnell et al. for temperatures up to 1273 K (assuming $\nu = 0.28$). Larsen and Adams [45] have reported a value of $G = 1.3 \times 10^5$ MPa at 1748 K indicating that the linear extrapolation technique is an acceptable method for estimating the shear modulus in the temperature range 1573 K - 1673 K. Using the extrapolated shear modulus data of Kossowsky et al., a plot of $\dot{\varepsilon} G^{n-1} T$ versus 1/T was constructed giving a true activation energy of 692 $\pm$ 25 kJ mol^{-1}. This activation energy is in excellent agreement with activation energy data for silicon nitride, summarized in Table AIII of reference 23, with additional data in references 1, 20 and 25.

4.3 Identification of the Rate Controlling Mechanism

The majority of the creep deformation studies of hot pressed, sintered, hot isostatically pressed and reaction bonded silicon nitride have determined

the stress exponent, n, to be approximately 2, and the activation energy of the rate controlling mechanism to be in the range 600 - 750 kJ mol^{-1}. Grain boundary sliding is observed in the amorphous grain boundary phase, accompanied by microcrack development [19,29]. It has been suggested that deformation is strongly dependent on the viscosity of the grain boundary phase, the silicon nitride dissolution and reprecipitation reactions and the transfer of the viscous phase from boundaries under compression to those in tension [19,29]. It is well established that additives such as CaO, which cause a marked reduction in the softening point and viscosity of silica glass, increase the creep strains and deformation rates of hot pressed silicon nitride [1,17,19,29].

The existing creep data for silicon nitride fall into two groups: (a) data collected in the temperature range 1523 K - 1673 K, where well defined steady state creep rates have been observed, as in the present study; and (b) data collected at lower temperatures 1373 K - 1523 K, where only primary creep has been observed. Activation energies determined from the steady state data lie in the range 650 - 750 kJ mol^{-1} and will now be compared with existing diffusion data for silicon nitride, and activation energies from primary creep and oxidation studies.

The self diffusion coefficients for nitrogen in single crystal grains of polycrystalline alpha- and beta-silicon nitride have been measured by Kijima and Shirasaki [48], giving values of 235 kJ mol^{-1} and 778 kJ mol^{-1} respectively. Although the value for β-Si_3N_4 is only 78 kJ mol^{-1} higher than the value of 700 kJ mol^{-1}, measured in the present study, it is unlikely that bulk diffusion of nitrogen would be rate controlling in the presence of a continuous, amorphous grain boundary phase. However, very limited diffusion data are available for these grain boundary phases. Wötting [1,49] reports values for Si/N diffusion in the grain boundary phase of hot pressed silicon nitride

of (a) 448 kJ mol^{-1} at temperatures below 1823 K and (b) 695 kJ mol^{-1} at temperatures above 1823 K (for 10 wt% Y_2O_3 additive); and (c) 645 kJ mol^{-1} (for 5 wt% MgO additive - temperature range not indicated).

The primary creep studies give a wider range of activation energy values. Arons and Tien [31], in agreement with Lange et al. [41], concluded that permanent creep and viscoelastic deformation were parallel processes which could be treated independently. Activation energies of 403 $\pm$ 113 kJ mol^{-1} (at constant strain (0.9%)) and 848 kJ mol^{-1} (at constant time (10 h)), were determined by Arons and Tien for three point bend tests of NC-132 (MgO additive) in the temperature range 1450 K - 1533 K. Tests at constant structure were carried out by temperature jump experiments on a single specimen with significant creep strain, giving an activation energy of 819 $\pm$ 84 kJ mol^{-1}, which confirmed the value of 848 kJ mol^{-1} determined above. The activation energy for the viscoelastic process was obtained through the temperature dependence of the recovery rate (taken 4 h after load removal) and was found to be 722 kJ mol^{-1}. Arons and Tien concluded that the persistent creep deformation occured by grain boundary sliding accomodated by grain boundary phase percolation and cavitation void and wedge opening.

A study of both primary creep and the oxidation kinetics of $70Si_3N_4$-$25SiO_2$-$5Y_2O_3$ (mol%) has been conducted by Bouarroud et al. [25]. They showed that oxidation occurred in the intergranular glass phase with activation energies of 146 $\pm$ 15 kJ mol^{-1} and 680 $\pm$ 80 kJ mol^{-1}, for the temperature ranges 1453 K - 1693 K and 1693 K - 1923 K, respectively. In the lower temperature regime, they suggested that the inward diffusion of oxygen could be the limiting step, whereas at higher temperatures, the outward diffusion of an "yttrium-nitrogen" compound species was thought to be the limiting step. The oxidation data was related to the creep data by using the strain rates at

constant degree of oxidation (i.e. constant weight gain) to determine the activation energy. It should be noted that no grain growth was observed in this material. Irrespective of the weight gain value selected, an activation energy of 720 kJ mol^{-1} was determined. This value is identical to that determined by Tien for the viscoelastic process and is very close to the value of 700 kJ mol^{-1} measured in the present study.

Bouarroud et al. modelled the primary creep strain, ε, as the sum of the viscoelastic component, ε_v, and the diffusional component, ε_d, giving

$$\varepsilon = \varepsilon_v + \varepsilon_d \tag{6}$$

and

$$\dot{\varepsilon} = \dot{\varepsilon}_v + \dot{\varepsilon}_d \tag{7}$$

From the analysis of Lange et al. [41], the creep rate was written as:

$$\dot{\varepsilon} = \frac{1}{\eta} f(S_v,\sigma) + S_d\, \sigma \exp(-E_d/RT) \tag{8}$$

where η = viscosity of the grain boundary phase; S_v depends on the structural state of the material, $S_v(S_o,D,E,A)$; S_o = thickness of the glassy interphase; D = mean grain size; E = elastic modulus of a grain boundary asperity; A = areas of the asperity; σ = applied stress; S_d depends on the structural state; and E_d = activation energy of the diffusional mechanism.

An Arrhenhius expression was assumed for the viscosity giving;

$$\dot{\varepsilon} = \frac{1}{\eta_o} f(S_v,\sigma) \exp(-E_v/RT) + S_d\, \sigma \exp(-E_d/RT) \tag{9}$$

where E_v is the activation energy of the glass viscosity.

The experimental observation that the activation energy measured was constant for all weight gains, led Bouarroud et al. to the conclusion that E_v must be equal to E_d and that matter transport through the glassy phase was the rate limiting step.

4.4 Relationship between the viscosity and diffusivity of a liquid

The above conclusion can be reconciled with the activation energy values obtained by (a) Arons and Tien, (b) in the present study, and (c) in silicon nitride containing magnesia or yttria additives, when the Einstien relationship between the mobility of a liquid and its diffusivity is introduced [50]. The resistance, F, suffered by a small sphere of liquid of radius a, moving with an average velocity, $\bar{v}$, with respect to the surrounding particles is given by Stokes' law:

$$F = 6 \pi a \eta \bar{v} \tag{10}$$

This can be written as

$$\bar{v} = \alpha F \tag{11}$$

where α is the mobility of the particle, given by

$$\alpha = \frac{1}{6 \pi a \eta} \tag{12}$$

According to Einstein's theory of Brownian motion

$$\alpha = \frac{D}{k T} \tag{13}$$

where D is the self diffusion coefficient of the liquid, k = Boltzmann's constant, T = temperature (K).

Hence
$$\eta = \frac{k T}{6 \pi a D} \tag{14}$$

and if
$$D = D_o \exp (-E_d'/kT) \tag{15}$$

where E_d' is equivalent to E_d in Equation (9)

then
$$\eta = \frac{k T}{6 \pi a D_o} \exp (E_d'/kT) \tag{16}$$

showing that the activation energy for the viscosity is the same as that for the self diffusion of the liquid.

The kinetic theory for the viscosity of liquids was developed by Frenkel in 1926 [51] and is discussed in detail in reference [52].

4.5 The role of additives

In deriving the relationship between the viscosity and self diffusivity of a liquid (Eqn. (16), Frenkel assumed that the average resistance of the liquid to the motion of one of its particles could be determined by Stokes law [39]. If a particle of the liquid is replaced by a particle of a foreign substance dissolved in the liquid, then by Stokes law, there will be very little change in the mobility for the foreign particle unless there is a large difference in the radii of the particles. Hence the diffusion coefficients of the different dissolved species must be approximately equal to each other and to the self-diffusion coefficient of the solvent.

This concept can be applied to silicate glasses by assuming that the various "particle sizes" are associated with the silica tetrahedra and the diffusing ions. The circumscribed sphere for the silica tetrahedron has a radius of 0.152 nm compared to the following radii for the respective ions: 0.171 nm - N^{3-}; 0.14 nm - O^{2-}; 0.065 nm Mg^{2+}; 0.099 nm - Ca^{2+}; 0.05 nm - Al^{3+}; 0.093 nm - Y^{3+}; 0.041 nm - Si^{4+}. It should be noted that the circumscribed sphere for the silica tetrahedon was determined using the ionic radii modified by the coordination number (CN), i.e. O^{2-} = 0.114 nm (CN 2) and Si^{4+} = 0.038 (CN 4) [53-56]. Hence, there is little difference between the radii of the diffusing species, with the radius of the nitrogen ion, N^{3-}, being the largest. This result suggests that the diffusion of the nitrogen ion may be the rate controlling mechanism, as discussed below in the context of the oxidation mechanism.

The correlation between viscosity and diffusivity has been investigated by Schaeffer for vitreous silica [57-59]. He concluded that the diffusivity of

silicon or the SiO_4 tetrahedron was rate controlling for viscous flow phenomena involving the silica phase, such as the high temperature creep of ceramic materials with silica-rich grain boundaries. However, he noted that the oxidation data of Si_3N_4 differed from those for Si, $MoSi_2$ and SiC and suggested that the release of nitrogen at the Si_3N_4/SiO_2 interface may be responsible. Further research is now required to determine whether the two phase regions observed in the glass phase of Si_3N_4-$6Y_2O_3$-$2Al_2O_3$ correspond to the presence of (a) nitrogen rich glass; (b) oxygen rich glass; or (c) nitrogen gas bubbles; in order to clarify the rate controlling mechanism.

4.6 Relationship between the creep mechanism and oxidation

When silicon nitride is creep tested in air, passive oxidation, at high oxygen levels in the atmosphere, results in a protective SiO_2 rich layer forming at the surface, according to the reaction:

$$Si_3N_4\ (s) + 3O_2\ (g) \rightarrow 3SiO_2\ (s) + 2N_2\ (g) \qquad (17)$$

In magnesia-fluxed materials it has been shown that the chemical potential gradient established results in an increase of the magnesium ion concentration in the surface scale. Diffusion of the magnesium cations from the bulk to the surface was proposed as the rate controlling mechanism for oxidation [60,61]. Similarly, Bouarroud et al. [25] reported segregation of yttrium to the subscale during oxidation of $70Si_3N_4$-$25SiO_2$-$5Y_2O_3$, but concluded that the limiting step was matter transport through the glassy grain boundary phase, possibly by a "yttrium-nitrogen compound" (complex).

In the present work, we conclude that the rate limiting step may be the transport of the nitrogen ions, rather than a complex species, through the grain boundary glassy phase to the surface as illustrated schematically in Fig. 8. The silicon nitride grains are shown surrounded by the glassy phase and exposed to air. At the surface, nitrogen ions in the glass give up electrons

and form nitrogen gas. This reaction can only occur if there is a species in the glass or the surrounding environment to accept the electrons. In this case oxygen atoms accept electrons, forming ions, with $6O^{2-}$ ions being formed for every $4N^{3-}$ converted to nitrogen gas. The oxygen anions will attach to available network cations, and once these are exhausted will induce a flux of cations from the bulk to the surface. This flux will include the cations in the glass, e.g. Y^{3+}, Mg^{2+}, Al^{3+} and also Si^{4+} ions from the dissolution of the silicon nitride. A parallel flux of nitrogen anions to the surface, also from the dissolution of the silicon nitride, will occur to replace the nitrogen ions evolved as nitrogen gas. Since N^{3-} has the largest ionic radius it is likely to have the slowest diffusivity, resulting in nitrogen ion transport through the glassy phase being the rate limiting step.

4.7 Interpretation of Creep Data

The above mechanistic interpretation can provide a satisfactory explanation for much of the creep data available for silicon nitride.

(1) The activation energies measured for creep of silicon nitride fall within the range 600 - 750 kJ mol^{-1} irrespective of the type of additive, since nitrogen transport is the rate limiting step in each case.

(2) The creep mechanism is identical for the primary and steady state studies described above for the temperature ranges 1373 K - 1523K and 1523K - 1673 K, with the true steady state being reached when there is a constant flux of N^{3-} ions from the bulk to the surface.

(3) The creep rates of silicon nitride are much lower in helium environments since there is no surface species (e.g. O_2) to accept electrons, and the concentration of impurities, such as Fe^{3+}, which could change oxidation state is generally very low [29].

(4) The viscosity of the glass increases with time, i.e. a hardening effect is

observed during long term creep tests. This could be attributed to increasing nitrogen concentration levels in the oxynitride glass, rather than to the depletion of Mg^{2+} or Y^{3+}. For example, Drew et al. [62] have established a correlation between increasing viscosity and increasing nitrogen levels in series of oxynitride glasses of constant metal atom content.

(5) Once crystallization of the glassy phase occurs, matter transport through the crystalline regions will become important, and the activation energy and rate limiting mechanism for the creep process must change. Activation energies may change continuously with temperature reflecting the increased degree of crystallization in the grain boundary phase.

(6) The strain rate derived by Evans and Rana [43] for a material with a continuous grain boundary phase

$$\dot{\varepsilon} = \omega \sigma_\infty^2 E^{-1} \exp(-Q_\eta/RT) \qquad (18)$$

where ω = constant, σ_∞ = remote stress, E = Young's modulus, Q_η = activation energy for the viscous mechanism

can now be replaced by

$$\dot{\varepsilon} = \omega' \sigma_\infty^2 E^{-1} \exp(-Q_D/RT) \qquad (18)$$

where ω' = constant and Q_D = activation energy for diffusion through the grain boundary phase.

Hence creep can be shown to occur by a diffusion controlled mechanism with a stress exponent, n = 2.

5. CONCLUSIONS

1. The creep properties of Si_3N_4-$6Y_2O_3$-$2Al_2O_3$, prepared by a two stage gas pressure sintering process, have been determined in the temperature range 1573 K - 1673 K, giving a stress exponent, n = 2.00 $\pm$ 0.15 and a true activation energy of 692 $\pm$ 25 kJ mol^{-1}.

2. The creep exponent, n = 2, can be rationalized in terms of Newtonian viscous sliding accompanied by microcrack formation and cavitation.

3. The viscosity of the grain boundary phase has the same activation energy as that for the self diffusion of the liquid, when Einstein's relationship between the mobility and the diffusivity of a liquid is introduced.

4. The activation energy is consistent with a diffusion controlled mechanism, with the rate controlling mechanism being the transport of nitrogen ions through the grain boundary phase.

5. The mechanistic interpretation proposed provides an explanation for the role of (a) additives; (b) helium environments; (c) observed viscosity changes; and (d) crystallization, during the creep testing of silicon nitride ceramics.

ACKNOWLEDGEMENTS

This research was supported by the National Aeronautics and Space Administration under grant number NASA NAG 3-685. The authors would like to thank the AiResearch Casting Company of the Garrett Corporation for supplying the material; Dr. Hun Yeh of the AiResearch Casting Company and Dr. A. Chokshi, U. C. Davies, for many helpful discussions during this research; and Karrel de la Cruz for assistance with the creep tests. Zhi-Yue Xu was supported as a visiting scholar by the South-West Petroleum Institute, Peoples' Republic of China, and by the National Oceanic and Atmospheric Agency through the USC Sea Grant Program. This research was funded in part by (a) an appointment (J. A. Todd) to the U. S. Department of Energy Faculty Research Participation Program (1986) administered by Oak Ridge Associated Universities; and (b) the Basic Energy Sciences Division, USDOE, through the SHaRE program under contract DE-AC05-76OR00033 with Oak Ridge Associated Universities. The authors gratefully acknowledge all the above support.

REFERENCES

1. G. Ziegler, J. Heinrich and G. Wötting, J. Mater. Sci. **22** (1987) 3041.
2. G. G. Deely, J. M. Herbert and N. C. Moore, Powder Metall. **8** (1961) 145.
3. Y. Oyama and O Kamigaito, Jpn. J. Appl. Phys. **10** (1971) 1637.
4. G. E. Gazza, J. Am. Ceram. Soc. **56** (1973) 662.
5. I. C. Huseby and G. Petzow, Powder Met. Int. **6** (1974) 17.
6. H. Hausner, Sci. Ceram. **12** (1983) 229.
7. K. S. Mazdiyasni and C. M. Cooke, J. Am. Ceram. Soc. **57** (1974) 536.
8. S. H. Knickerbocker, A. Zangvil and S. D. Brown, J. Am. Ceram. Soc. **68** (1985) C99.
9. D. R. Clarke and G. Thomas, J. Am. Ceram. Soc. **60** (1977) 491.
10. O. L. Krivanek, T. M. Shaw and G. Thomas, J. Am. Ceram. Soc. **62** (1979) 585.
11. L. K. V. Lou, T. E. Mitchell and A. H. Heuer, J. Am. Ceram. Soc. **61** (1978) 392.
12. A. Tsuge and K. Nishida, J. Am. Ceram. Soc. **58** (1975) 323.
13. A. Tsuge and K. Nishida, Am. Ceram. Soc. Bull. **57** (1978) 424.
14. D. R. Clarke and G. Thomas, J. Am. Ceram. Soc. **61** (1978) 114.
15. C. C. Ahn and G. Thomas, J. Am. Ceram. Soc. **66** (1983) 14.
16. F. F. Lange, Int. Met. Rev. **1** (1980) 1.
17. S. Ud Din and P. S. Nicholson, J. Mater. Sci. **10** (1975) 1375.
18. J. M. Birch and B. Wilshire, J. Mater. Sci. **13** (1978) 2627.
19. P. J. Dixon-Stubbs and B. Wilshire, J. Mater. Sci. **14** (1979) 2773.
20. J. Heinrich and M. Böhmer, Ber. Dtsch. Keram. Ges. **61** (1984) 399.
21. C. L. Quackenbusch, J. T. Smith, J. T. Neil and K. W. French, in "Progress in Nitrogen Ceramics", edited by F. L. Riley, (Martinus-Nijhoff, 1983) p. 669.

22. L. J. Bowen, T. J. Carruthers and R. J. Brook, J. Am. Ceram. Soc. **61** (1978) 335.

23. W. R. Cannon and T. G. Langdon, J. Mater. Sci. **18** (1983) 1.

24. W. R. Cannon and T. G. Langdon, J. Mater. Sci. **23** (1988) 1.

25. A. Bouarroud, J. P. Goursat and J. L. Besson, J. Mater. Sci. **20** (1985) 1150.

26. G. Q. Weaver and J. W. Lucek, Am. Ceram. Soc. Bull. **57** (1978) 1131.

27. G. W. Hollenberg, G. R. Terwilliger and R. S. Gordon, J. Amer. Ceram. Soc. **54** (1971) 196.

28. G. Leng-Ward and M. H. Lewis, Mat. Sci. Eng. **71** (1985) 101.

29. R. Kossowsky, D. G. Miller and E. S. Diaz, J. Mater. Sci. **10** (1975) 983.

30. M. S. Seltzer, Ceram. Bull. **56** (1977) 418.

31. R. M. Arons and J. K. Tien, J. Mater. Sci. 15 (1980) 2046.

32. C. K. L. Davies and S. K. Sinha Ray, in "Special Ceramics" edited by P. Popper, (British Ceramic Research Association, Stoke-on-Trent, 1972), p. 193.

33. R. Kossowsky, in "Ceramics for High-Performance Applications", edited by J. J. Burke, A. E. Gorum and R. N. Katz, (Brook Hill, Chestnut Hill, Massachusetts, 1974), p. 347.

34. J. A. Mangels, ibid, p. 195.

35. W. Engel, E. Gugel and F. Thümmler, in "Science of Ceramics", Vol. 7 (Societé Francaise de Céramique, Paris, 1976), p. 415.

36. J. M. Birch, B. Wilshire, D. J. R. Owen and D. Shantaram, J. Mater. Sci. **11** (1976) 1817.

37. J. M. Birch, B. Wilshire and D. J. Godfrey, Proc. Brit. Ceram. Soc. **26** (1978) 141.

38. G. Grathwohl and F. Thümmler, J. Mater. Sci. **13** (1978) 1177.

39. P. K. Talty and R. A. Dirks, J. Mater. Sci. **13** (1978) 580.

40. G. Grathwohl and F. Thümmler, Ceramurgia Int. **6** (1980) 43.

41. F. F. Lange, B. I. Davis and D. R. Clarke, J. Mater. Sci. **15** (1980) 601.

42. J. A. Palm and C. D. Greskovich, Bull. Amer. Ceram. Soc. **59** (1980) 447.

43. A. G. Evans and A. Rana, Acta Metall. **28** (1980) 129.

44. D. A. Bonnell, T. Y. Tien, M. Lee and M. K. Brun, in 2nd. Int. Conf. Science Hard Mater., Inst. Phys. Conf. Ser. No. 75, (Adam Hilger Ltd., 1986) p. 401.

45. D. C. Larsen and J. W. Adams, "Property Screening and Evaluation of Ceramic Turbine Materials: Semiannual Report No. 8, June 1980, USAF Contract F33615-C-5100, pp. 22, 55.

46. R. R. Wills, R. W. Stewart and J. M. Wimmer, Cer. Bull. **56** (1977) 194.

47. W. A. Fate, J. Am. Ceram. Soc. **57** (1974) 49.

48. K. Kijima and S. Shirasaki, J. Chem. Phys. **65** (1976) 2668.

49. G. Wötting, Thesis, TU Berlin, (1983).

50. A. Einstein, Annalen der Physik **19** (1905) 371.

51. J. Frenkel, Z. f. Phys. **35** (1926) 652.

52. J. Frenkel, "Kinetic Theory of Liquids" (Dover, N.Y. 1955) p. 191.

53. L. H. Van Vlack, "Elements of Materials Science and Engineering", Fifth Edition, (Addison Wesley, 1985) p. 48.

54. A. R. West, "Solid State Chemistry and its Applications" (John Wiley, 1984) p.271.

55. R. D. Shannon and C. T. Prewitt, Acta Cryst. **B25** (1969) 725.

56. R. D. Shannon and C. T. Prewitt, Acta Cryst. **B26** (1970) 1046.

57. H. A. Schaeffer, "Encyclopedia of Materials Science and Engineering" edited by M. B. Bever (Pergamon Press, 1986) p. 4396.

58. H. A. Schaeffer, J. Non-Cryst. Solids **38/39** (1980) 545.

59. H. A. Schaeffer, J. Non-Cryst. Solids **67** (1984) 19.

60. D. R. Clarke, in "Progress in Nitrogen Ceramics", edited by F. L. Riley, (Martinus-Nijhoff, 1983), 421.

61. P. Vincenzini and A. Babini, in "Sintered Metal-Ceramic Composites", edited by G. S. Upadhyaya (Elsevier, Amsterdam, 1984), 425.

62. R. Drew, S. Hampshire and K. H. Jack, in "Progress in Nitrogen Ceramics" edited by F. L. Riley (Martinus-Nijhoff, 1983) 323.

FIGURES

Fig. 1 The variation of creep strain (%) with time for Si_3N_4-$6Y_2O_3$-$2Al_2O_3$ tested at 1673 K and an applied stress of 36.4 MPa.

Fig. 2 Creep strain rate versus strain (%) for specimens tested at 1673 K and applied stresses in the range 10.4 MPa - 52 MPa.

Fig. 3 Steady state creep strain rate versus applied stress for temperatures of 1573 K, 1623 K and 1673 K. (A) and (B) represent specimens taken from different groups in the same batch process.

Fig. 4 The variation in steady state creep strain rate with reciprocal temperature for Si_3N_4-$6Y_2O_3$-$2Al_2O_3$ deformed at 50 MPa. $Q = 700 \pm 25$ kJ mol^{-1}.

Fig. 5 Transmission electron micrographs of the as-sintered Si_3N_4-$6Y_2O_3$-$2Al_2O_3$

(a) A - β-Si_3N_4 grain with aspect ratio greater than 5, B - equiaxed grains

(b) C - continuous glassy phase surrounding silicon nitride grains.

Fig. 6 Scanning electron micrographs of specimen creep deformed for 1.5 h at 1673 K with an applied stress of 36.4 MPa.

(a) polished, unetched tensile surface showing microcracks and cavities

(b) thermally etched side of the specimen showing region of incomplete sintering

(c) and (d) fracture surface showing small voids and cracks.

Fig. 7 Transmission electron micrograph of specimen creep deformed for 22.4 h at 1673 K and a stress of 19.9 MPa

(a) A - grain boundary sliding, B - dislocation activity, C - phase separation within the glass

(b) Deformation in the glassy phase at grain boundaries, with meniscus formation at regions labelled D.

Fig. 8 Schematic representation of the oxidation and reduction reactions accompanying the creep deformation of Si_3N_4-$6Y_2O_3$-$2Al_2O_3$ when tested in air.

ORNL-DWG 86-13867

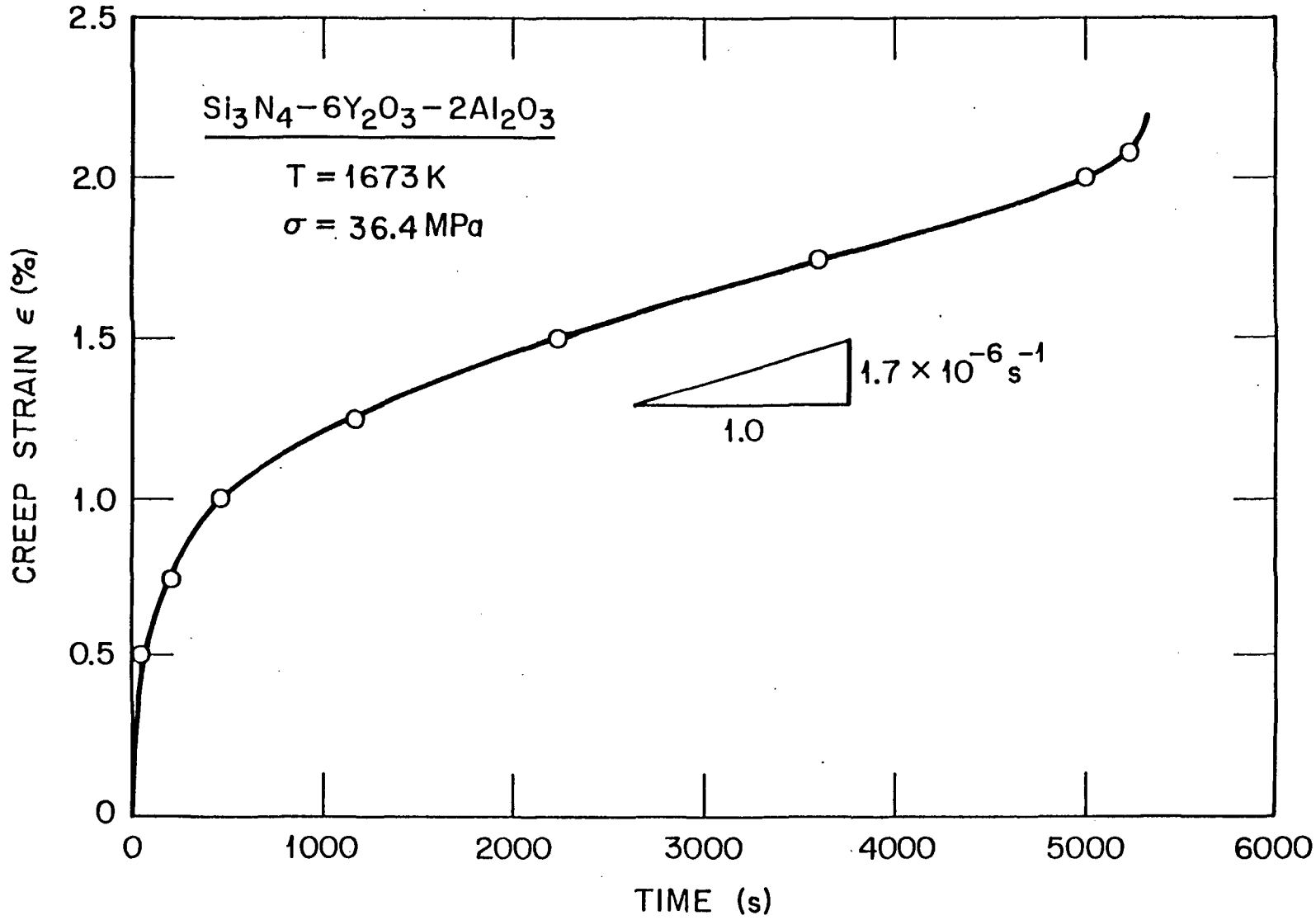

Fig. 1

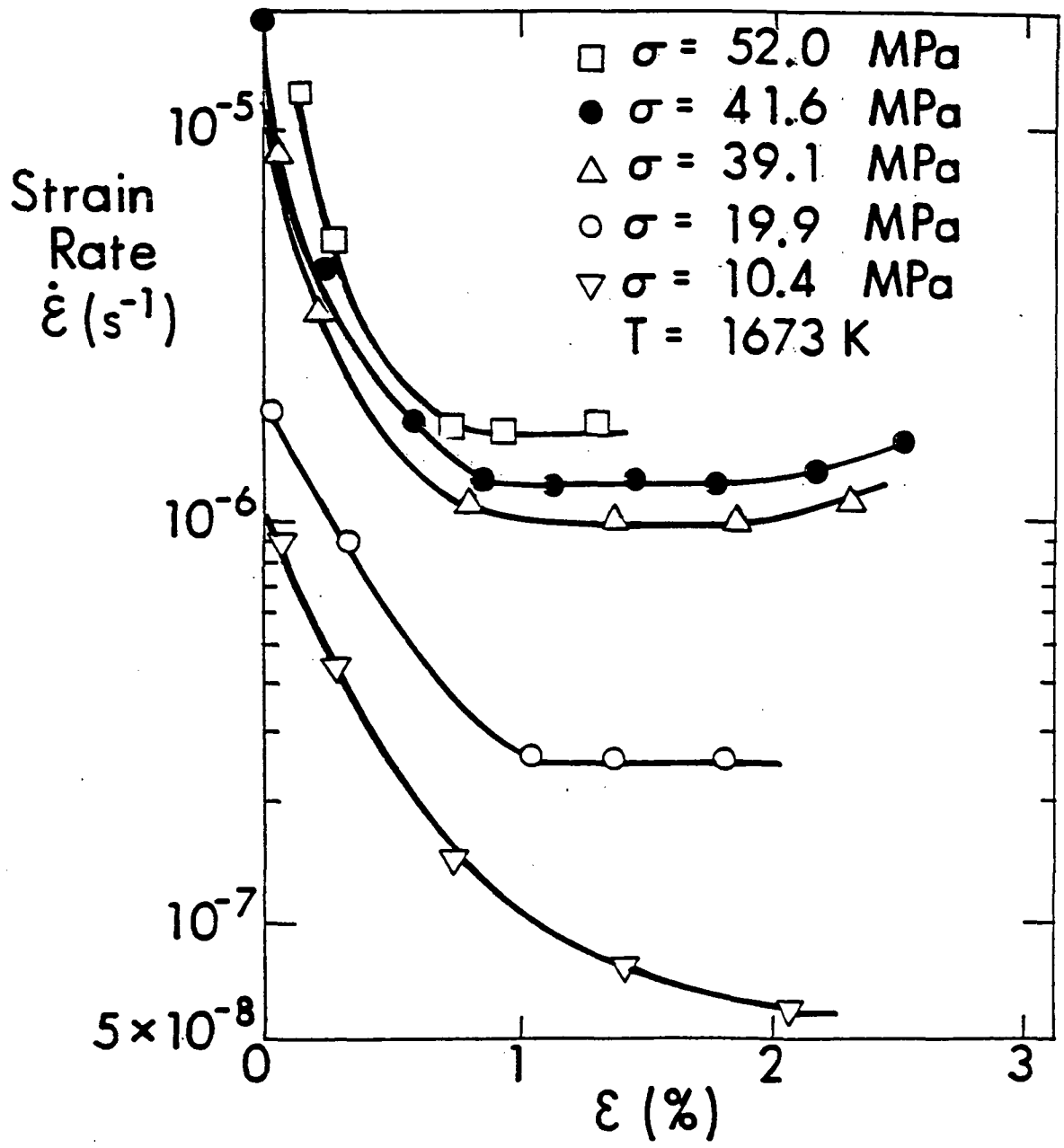
□ σ = 52.0 MPa
● σ = 41.6 MPa
△ σ = 39.1 MPa
○ σ = 19.9 MPa
▽ σ = 10.4 MPa
T = 1673 K
Strain Rate ε̇ (s⁻¹)
10⁻⁵
10⁻⁶
10⁻⁷
5×10⁻⁸
0
1
2
3
ε (%)

Fig. 2

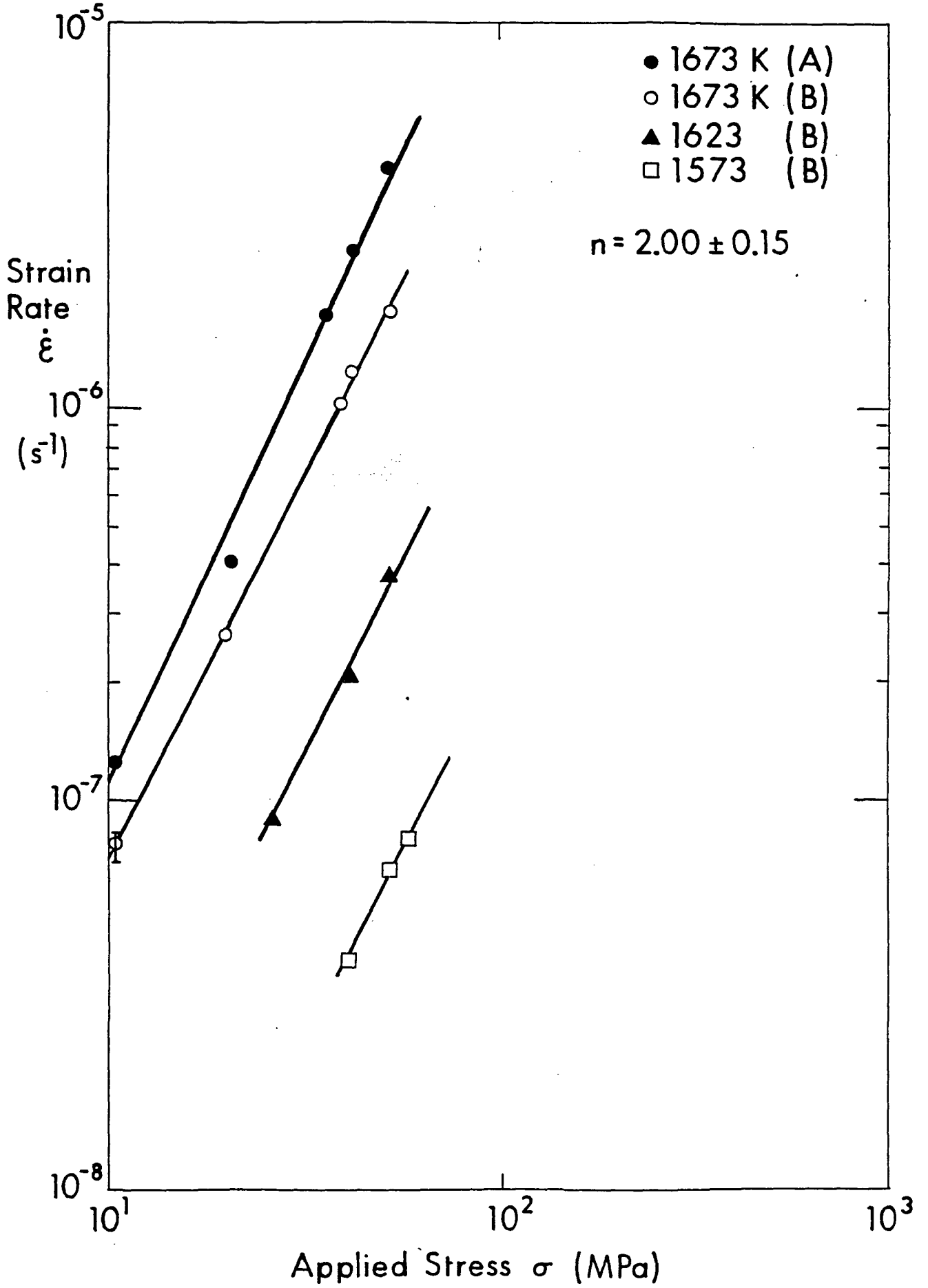
10^-5
10^-6
10^-7
10^-8
Strain Rate ε̇ (s^-1)
● 1673 K (A)
○ 1673 K (B)
▲ 1623 (B)
□ 1573 (B)
n = 2.00 ± 0.15
10^1
10^2
10^3
Applied Stress σ (MPa)

Fig. 3

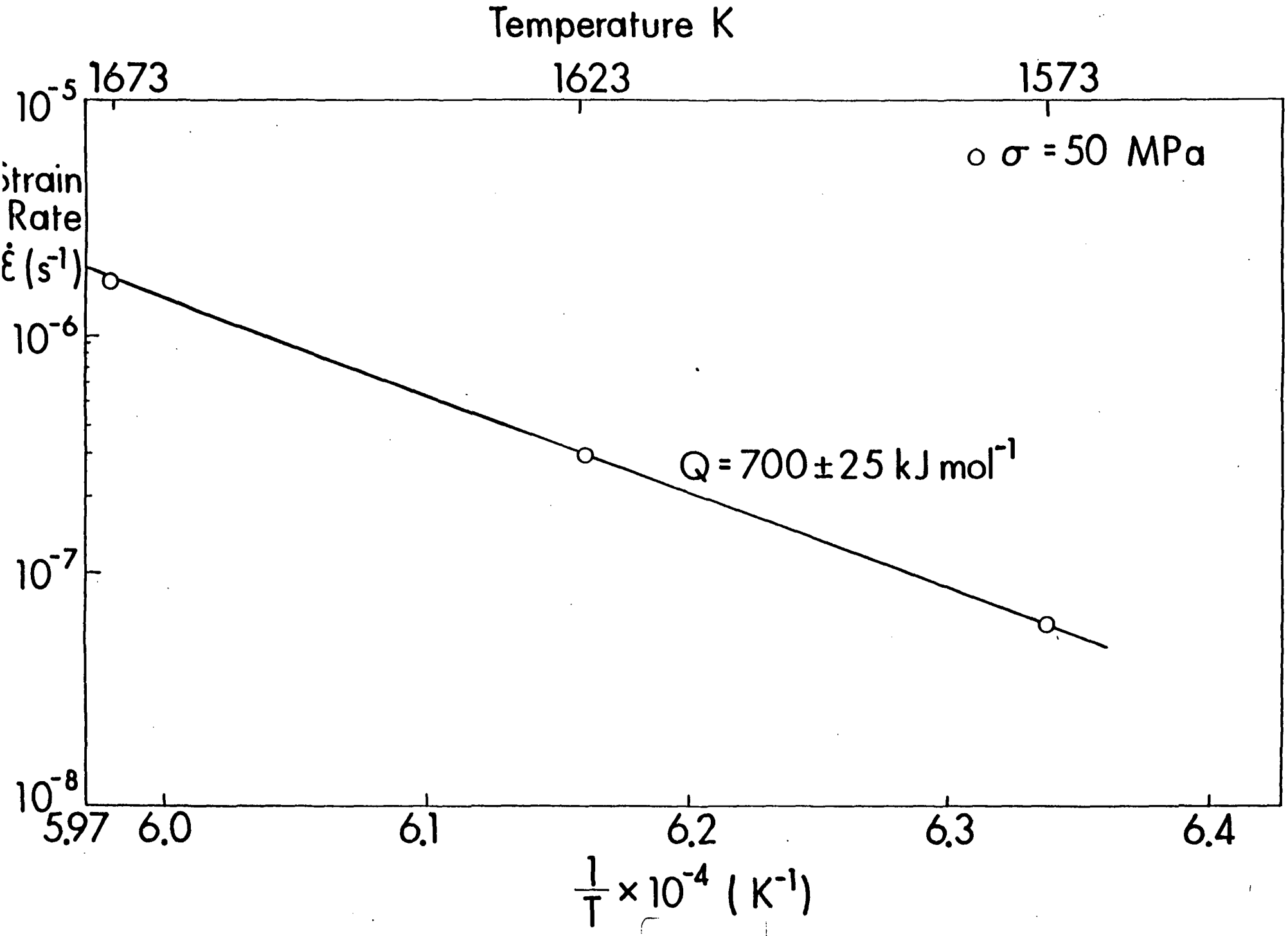
Temperature K
1673
1623
1573
10^{-5}
Strain Rate $\dot{\varepsilon}$ (s^{-1})
10^{-6}
10^{-7}
10^{-8}
o σ = 50 MPa
Q = 700 ± 25 kJ mol^{-1}
5.97
6.0
6.1
6.2
6.3
6.4
$\frac{1}{T} \times 10^{-4}$ (K^{-1})

Fig. 4

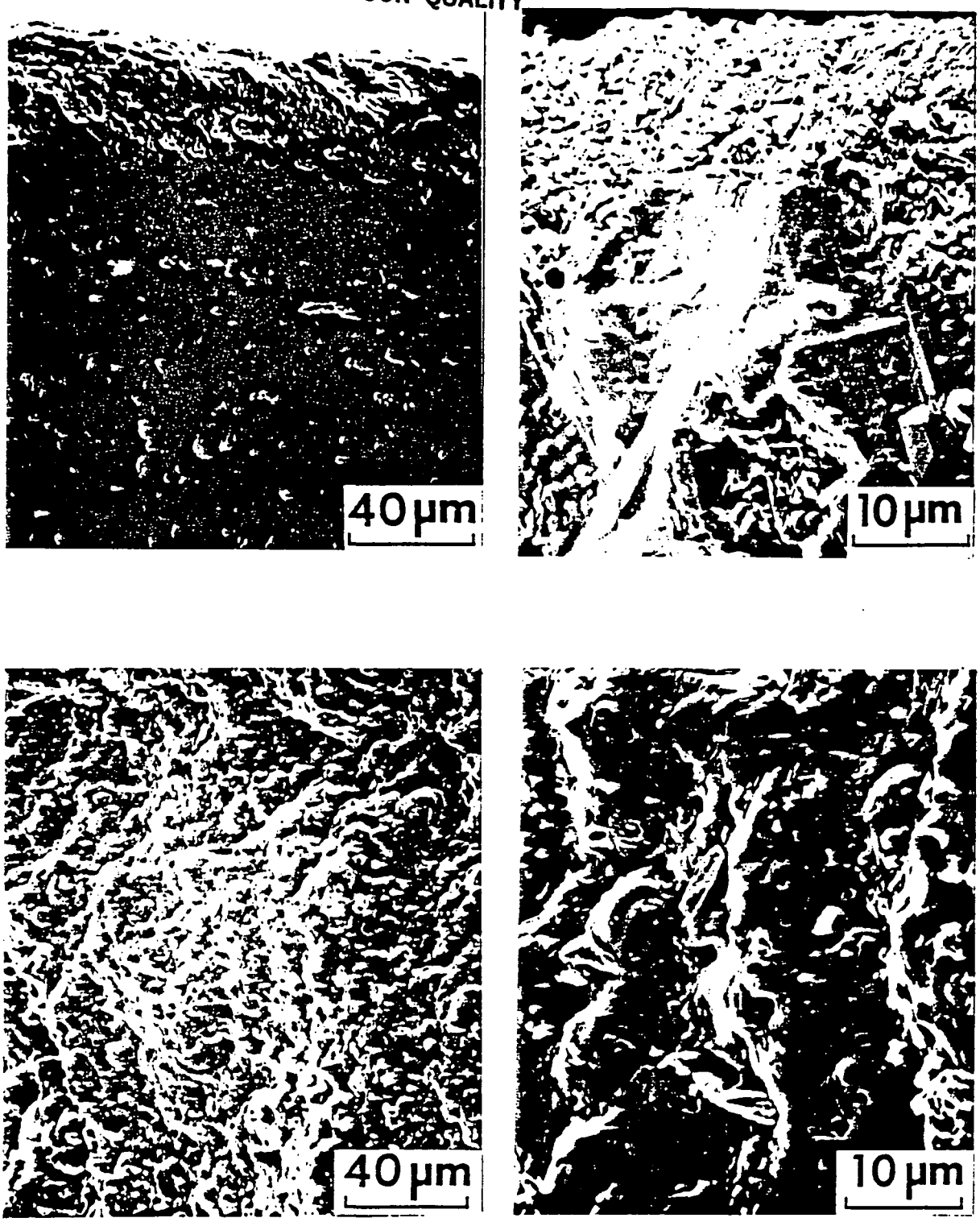

Fig. 5

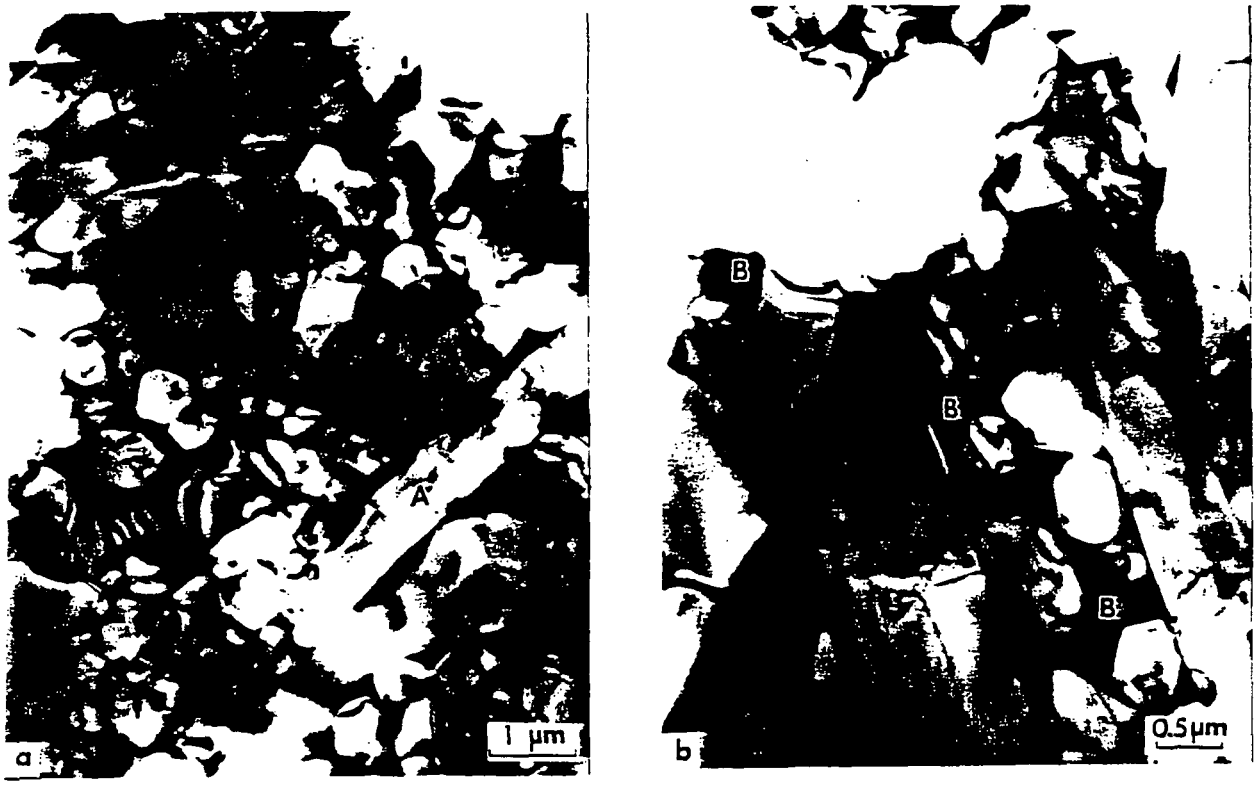

Fig. 6

Fig. 7

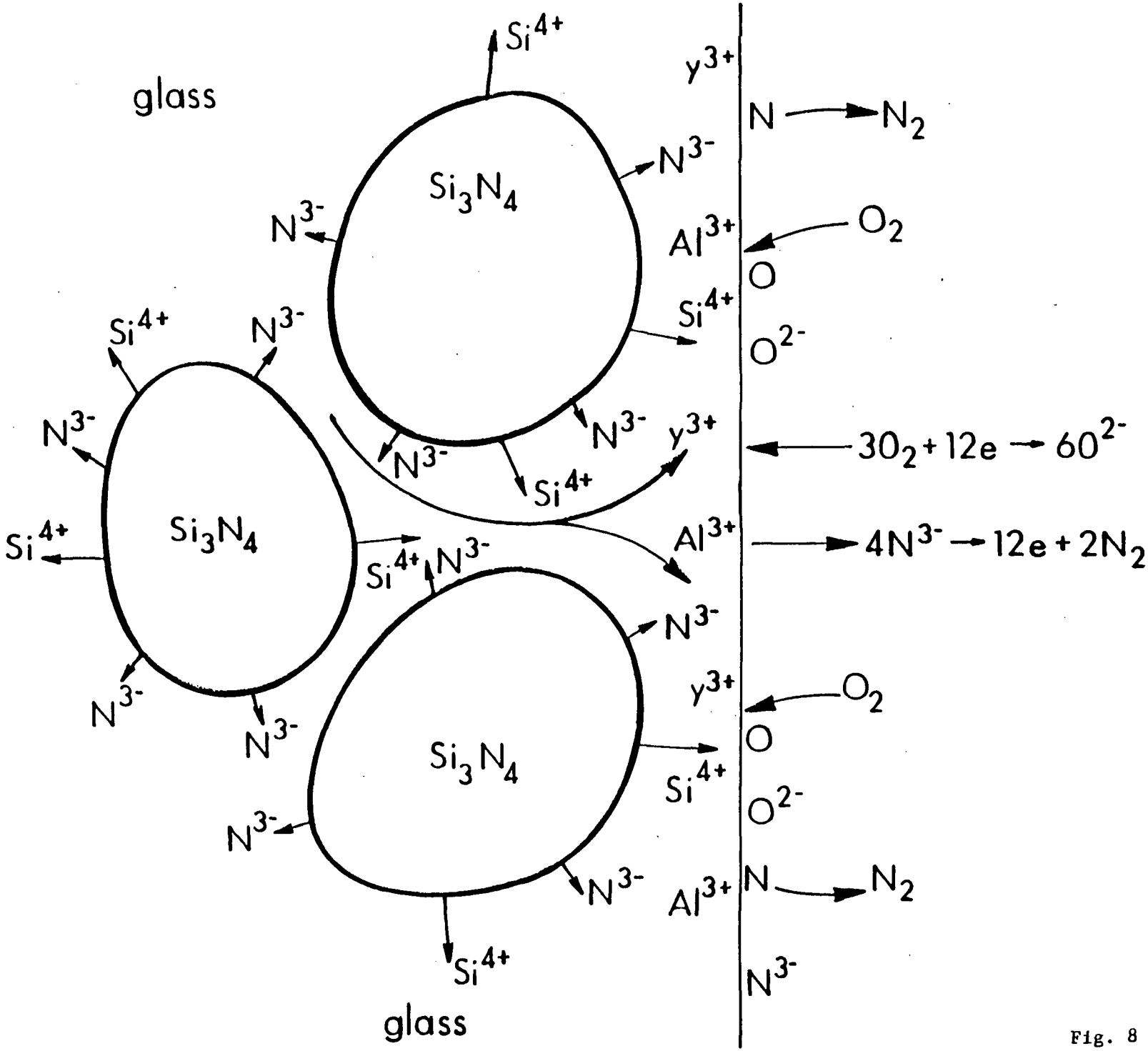
glass
Si^{4+}
y^{3+}
$N \rightarrow N_2$
N^{3-}
Si_3N_4
N^{3-}
Al^{3+}
O_2
O
Si^{4+}
O^{2-}
Si^{4+}
N^{3-}
N^{3-}
y^{3+}
$30_2 + 12e \rightarrow 60^{2-}$
N^{3-}
Si^{4+}
N^{3-}
Si^{4+}
Si_3N_4
Al^{3+}
$4N^{3-} \rightarrow 12e + 2N_2$
Si^{4+}
Si^{4+}
N^{3-}
N^{3-}
y^{3+}
O_2
N^{3-}
O
Si_3N_4
Si^{4+}
O^{2-}
N^{3-}
N^{3-}
Al^{3+}
$N \rightarrow N_2$
Si^{4+}
N^{3-}
glass

Fig. 8